Comparative Analysis on Semi-empirical Models of Jet Fire for Radiant Heat Estimation

Nur Shahidah Ab Aziz[1,2] · Rafiziana Md. Kasmani[1] · Mohd Dinie Muhaimin Samsudin[1] · Arshad Ahmad[3]

Abstract

Sudden release of combustible/flammable materials at high pressure could result in the occurrence of a jet fire in the processing industry. Understanding the jet fire phenomenon and its mechanism could assist practitioners and researchers to predict the radiant energy transfer caused by the jet fire. Due to the dynamics of jet fire occurrence, the development of a semi-empirical model to predict thermal characteristics in different scenarios might provide huge advantages to the industry and safety practitioners as it is nonexpensive and a reliable prediction. There are four semi-empirical models for jet fire thermal radiation estimation that has been developed to date, namely, solid flame model (SFM), single-point source model (PSM), multipoint source model (MPSM), and line source model (LSM). It is the aim of this paper to explore each model applicability and approach to estimate the radiant heat flux based on the governing factors associated with the models, i.e., atmospheric transmissivity, flame length, lift-off length, flame shape, radiant heat fraction, total heat release, and receiver location. It is found that the applicability of each model and the derived parameters are largely contributed by the flame scale (small, medium, and large), flame orientation, flame length, and flame shape as well as the flame distance to the target receiver. From the discussion made, it can be suggested that for both near- and far-field measurement, the weighted MPSM is a reliable model that can be used for both vertical and horizontal orientations with some modification upon the consideration of buoyancy effect. On another note, LSM is able to provide a better prediction for linear trajectory of jet flame; however, the applicability is still limited for jet flame trajectory with buoyancy effects due to fewer data available and validation in various release conditions and scenarios.

Keywords Jet fire · Thermal radiation · Semi-empirical model · Safety

Nomenclature

A_{IR}	2D area of the flame surface
c_2	Constant parameter c_p specific heat of air at constant pressure (kJ kg^{-1} K^{-1})
c_p	Specific heat of air at constant pressure (kJ kg^{-1} K^{-1})
C_x	Normalized incident radiation (q^{meas}/q^{model})
D_{eq}	Equivalent diameter of flame
d	Diameter of nozzle exit (mm)
d_{eff}	Effective diameter
d_j	Expanded jet diameter
E	Flame emissive power per area (kW m^{-2})
Fr	Froude number
f	Multiplying factor
f_s	Mass fraction of fuel at stoichiometric condition
G	Initial jet momentum flux
h_{RC}	Distance between the flame radiant center and the ground
H	Net calorific value of fuel (kJ kg^{-1})
L	Flame length from orifice (m)
L_0	Flame length with zero wind
L_b	Flame length in buoyancy region
L_c	Centerline flame length
L_f	Lift-off distance (m)
L_{IR}	Radiant flame length
L_m	Flame length in momentum region
L_n	Nozzle length
L_p	Projection distance
m	Mass flow rate (kg s^{-1})

✉ Rafiziana Md. Kasmani
    rafiziana@utm.my

1   Energy Management Research Group, School of Chemical and Energy Engineering, Faculty of Engineering, Universiti Teknologi Malaysia, 81310 Johor Bahru, Johor, Malaysia

2   Faculty of Chemical Engineering, Universiti Teknologi MARA, 40450 Shah Alam, Selangor, Malaysia

3   Institute of Future Energy, Universiti Teknologi Malaysia, 81310 Skudai, Johor, Malaysia

n_a	Stoichiometric air entrained	θ	Angle as shown in Fig. 4
$n(N)$	(Total) number of point sources	φ	Angle as shown in Fig. 4
P_a	Ambient pressure	ρ_j	Expanded jet density (kg m^{-3})
P_i	Initial pressure	ρ_s	Gas density at the jet exit
P_0	Stagnation pressure	ρ_∞	Ambient gas density
P_{out}	Pressure downstream of jet fire	γ	Ratio of specific heats
Q	Heat release rate (kW)	ξ	Richardson number
Q_R	Incident radiation		
Q_s^*	Dimensionless heat release rate		
$Q_{\zeta_l}^*$	Dimensionless heat release rate as defined in Eq. (19)		
Q_T	Net power of the flame (kW)		
$r(r_0)$	(Maximum) flame radius (m)		
R	Distance perpendicular to flame axis (m)		
Re	Reynolds number		
RH	Relative humidity of atmosphere (%)		
S	Distance from a point within the flame to the receiver (m)		
S_L	Maximum laminar burning velocity of the mixture under ambient conditions (m s^{-1})		
T	Temperature		
T_∞	Ambient air temperature		
$\overline{T}_{f,a}$	Mean flame temperature rise		
u	Velocity (m s^{-1})		
u_{eq}	Effective exit gas velocity of the gas jet		
U^*	dimensionless flow number		
u_j	Expanded jet velocity (m s^{-1})		
V	View factor		
W_o	Flame width		
W_n	Nozzle width		
x	Mass percentage		
X	Distance from the flame surface to exposed target (m)		

Abbreviations

EPPLL	Emissive power per line length
LSM	Line source model
MPSM	Multipoint source model
PSM	Single-point source model
SFM	Solid flame model

Greek symbols

α	Length ratio of lower flame to the whole flame
α_t	Tilt angle
α_w	Absorption factors (water vapor)
α_c	Absorption factors (carbon dioxide)
δ	Lift angle
δ_f	Laminar flame thickness under ambient conditions (m)
ε	Flame emissivity
σ	Stefan–Boltzmann constant (5.67×10^{-8} W m^{-2} K^{-4})
η	Fraction of heat radiated
η_H	Fraction of heat radiated in a horizontal orientation
η_m	Fraction of heat radiated of mixture
η_G	Fraction of heat radiated of gas
η_L	Fraction of heat radiated of liquid
η_V	Fraction of heat radiated in a vertical orientation
τ	Atmospheric transmissivity

Introduction

Fire can take many different forms. The hazards associated with fire are always in the form of radiant heat release. Fire can be remotely dangerous if the sources are not contained. There are three different forms of fire that can result from the release of gas or liquid hydrocarbon as illustrated in Fig. 1.

This study focuses on jet fire occurrence which is often associated with high momentum release, promoting air entrainment which elevates the combustion efficiency. In the event of jet fire, a gas flowing at internal pressure (P_{in}) influences the jet exit velocity, in which if the P_{in} increases, the jet exit velocity would increase until it reaches a maximum condition (velocity of sound in the gas). This condition is known as a sonic or choked flow. Most released gases reached sonic velocity if the release pressure is greater than 1.9 bar absolute. A choked condition is reached if the following criteria are fulfilled:

$$\frac{P_0}{P_{out}} \geq \left[\frac{2}{\gamma+1}\right]^{\frac{\gamma}{\gamma-1}} \tag{1}$$

where P_{in} is the internal pressure, P_{out} is the pressure downstream of the jet exit, and γ is the ratio of specific heats (Palacios Rosas 2011). In addition, jet fires always show turbulent characteristics, in which the flow could be chaotic and unstable due to internal and external factors as clearly illustrated in Fig. 2.

When jet fire occurred, the hazards result in the form of radiant heat transfer and the prediction of heat emission to the surrounding can be determined by semi-empirical models. In general, semi-empirical models offer the following advantages: they are easily programmed in the computer, repetitive calculation can be done in a short time, they are economical, and they could provide a reliable prediction based on theoretical principles and experimental observation. To date, semi-empirical models are adopted by industries and safety practitioners when conducting risk assessment for the plant and process. At present, four types of semi-empirical models are available, namely, solid flame model (SFM) (Raj 2007), point source model (PSM) (Hankinson and Lowesmith 2012), multipoint source model (MPSM) (Lowesmith and Hankinson 2013), and line source model (LSM) (Zhou and Jiang 2016). The models were developed based on factors
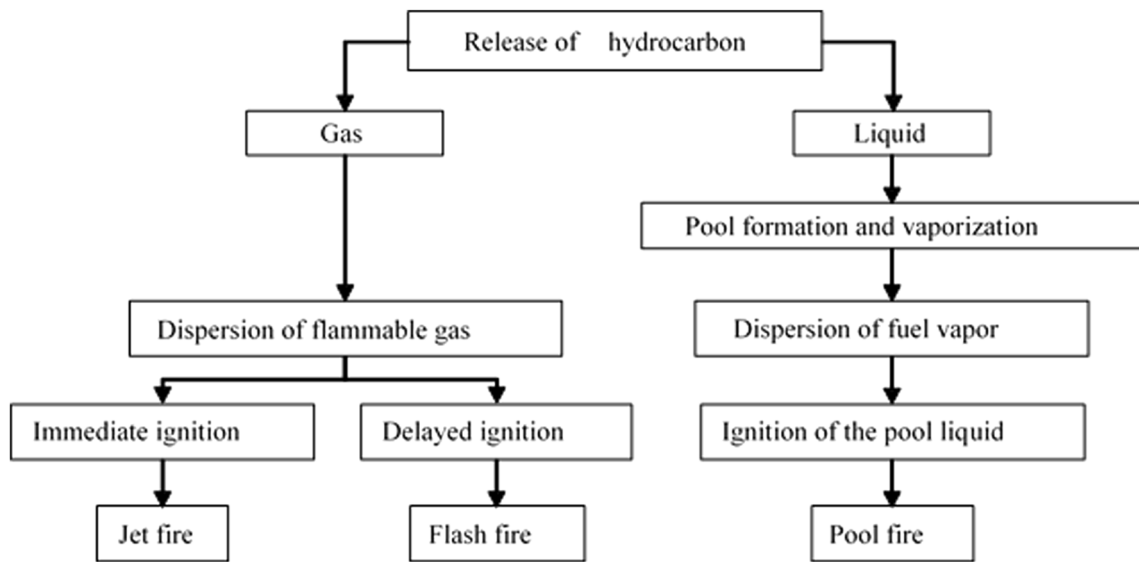
Fig. 1 Evolving of fire accident scenarios (Dadashzadeh et al. 2013)

including the jet flame shape, flame length, lift-off length, release flow rate, stagnant pressure, atmospheric transmissivity, release diameter, fuel reactivity, net heat release, and measurement distance. Since radiation heat transfer is the main subject during jet fire occurrence, the understanding on the physical and mechanism of jet fire and how each semi-empirical correlation relates with theories, fundamental equations, and assumptions will be our focal discussion in this paper. The governing parameters, physics, and dynamics of jet fires are reviewed for their applicability, and the present gaps between experiments as well as the common features on all models are discussed.

Semi-empirical Model of Jet Fire

The fundamental basis of radiant heat transfer estimation in a semi-empirical model is the size, shape, and relative orientation between two surfaces and their absorptivities and emissivities (Geankoplis 2003). Theoretically, the total emissive power E of radiation energy to a given surface for a black body is a relation of emissivity ε, Stefan–Boltzmann constant σ, and temperature T
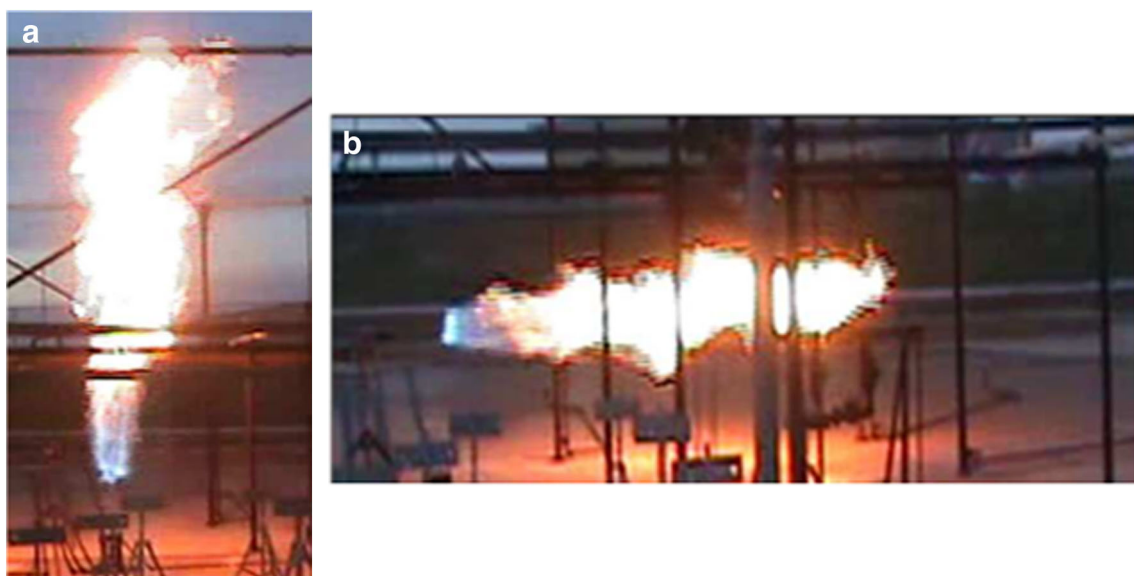
$$E = \varepsilon \sigma T^4 \tag{2}$$

Fig. 2 Jet fire release in **a** vertical and **b** horizontal orientation (Zhang et al. 2015)
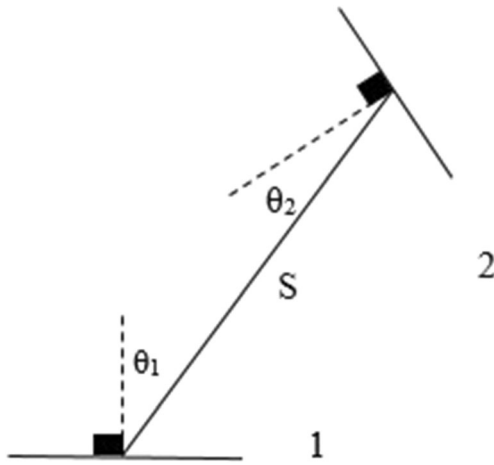
Fig. 3 Radiating power emitted from surface 1 to surface 2 at distance S

To understand the basic concept of energy flow from a hotter surface to a colder surface with intervention of media such as air, view factor V has been used to explain the phenomena. It can be defined as the energy exchange between two infinite parallel black plane and gray planes to a more complicated geometrical configuration as can be seen in Fig. 3.

Theoretically, view factor can be expressed as

$$\int_0^{A_1} \frac{\cos\theta_1\cos\theta_2}{\pi S^2} dA_1 \tag{3}$$

The basic equation involving the heat transfer between two infinite black planes is given in Eq. (4):

$$Q_R = VE \tag{4}$$

where Q_R is the radiant heat transfer, while V and E are the view factor and emissivity, respectively. With the presence of carbon dioxide and water vapor in air that act as absorbing media, thus, the transmissivity term τ shall be included in Eq. (4) that yield further equation that is adopted in the SFM:

$$Q_R = VE\tau \tag{5}$$

SFM is considered a well established model since the model is the most common method used by the industry for the consequence analysis. The applicability and suitability of each model—SFM, PSM, MPSM, and LSM—are varied,

depending on the process and geometrical factors. SFM and PSM are widely used models to estimate the radiant heat of fire. The shortcomings in terms of the field of observation factor for SFM and PSM models have been addressed in MPSM and LSM models and the explanation will be explored in the next section. It should be noted that all models developed are based on certain conditions that fit the models' best and on 1D basis. The governing equations of the said models are presented in Table 1.

Where Q_R is the radiant heat transfer, V is the view factor, E is the emissivity per flame area (kW m^{-2}), τ is the transmissivity, η is the fraction of heat radiated, Q_T is the total heat release, S is the measurement distance normal to the receiver surface area, E' is the emissivity per flame length (kW m^{-1}), and φ is the angle of measurement view normal to the receiver surface area. The said parameters of all models were obtained from experimental observation and theoretical assumptions. As such, emissivity E can be estimated by knowing the dimensions of the flame or via the value of η. The total heat flux Q_T is based on mass flow rate of released fuel m (kg s^{-1}) and net calorific value of the fuel H (kJ kg^{-1}), while radiant heat fraction η is based on radiant heat released Q_R over total heat release Q_T, while distance S and φ are based on the respective sensor location. Based on the aforementioned introduction, this paper attempts to discuss the parameters reported from experimental observations which are

i.   Field of observation.
ii. Geometrical features of flame that include flame shape, flame length, lift-off length, and width.
iii. Radiant heat fraction η is based on radiant heat released Q_R over total heat release Q_T.
iv. Atmospheric conditions.

General Applicability of Models in Near-Field and Far-Field Observation

A key aspect of a semi-empirical model for radiant heat estimation is the location of the receiver. Thus, to have a high accuracy of prediction, the field of observation is an important

Table 1 Semi-empirical model for radiant heat estimation for free-form jet fire

Model	Equation	
Solid flame model, SFM	$Q_R = VE\tau$	(6)
Single-point source model, PSM	$Q_R = \frac{\eta Q_T \tau}{4\pi S^2}$	(7)
Multipoint source model, MPSM	$Q_R = \sum_{j=1}^{N} \vec{Q}_j = \sum_{j=1}^{N} \frac{w_j \eta Q_T \tau_j}{4\pi \vec{S}_j^2} \cos\phi_j$	(8)
Line source model, LSM	$Q_R = \int_{L_f}^{L} \frac{\tau E'}{4\pi S^2} \cos\phi \, dz$	(9)

factor. In general, SFM is used for radiant heat prediction in near-field observation, while PSM is used in far-field observation in which the flame shape is not critical (Lowesmith and Hankinson 2012). Even though PSM can be used for both vertical and horizontal configurations of jet flame (Zhou et al. 2016), the applicability is limited to far field only (Hankinson and Lowesmith 2012; Lowesmith et al. 2007; Lowesmith and Hankinson 2012; Jujuly et al. 2015; Zhang et al. 2015) due to the fact that the model does not consider the flame shape in the radiant heat measurement (Hankinson and Lowesmith 2012). Not considering the effect of smoke, wind velocity, and direction is another major limitation of this model (Jujuly et al. 2015), leading to weak prediction on near-field radiation and convective flux. Figure 4 is the schematic diagram of PSM with two types of measurement distance to the receiver, S and R.

The gap experienced in the PSM model is addressed in MPSM. In MPSM, instead of assuming that radiant heat is emanated from one-point source, several points are taken, assuming that heat is radiated along the jet flame centerline. MPSM is a well-accepted model that is able to replicate data on both near- and far-field observations. Originally, there were three types of MPSM, namely, linear, curvilinear, and modified curvilinear. These models were fully described elsewhere (Crocker and Napier 1988). A simple MPSM is another type of MPSM. A model adopted by Hankinson and Lowesmith (2012), which is the weighted MPSM, has demonstrated good prediction on radiation heat released from vertical orientation on large-scale jet fire in the near field. For far-field radiation estimation, the model gives a reliable prediction within ± 20% tolerance compared to PSM (Hankinson and Lowesmith 2012). Besides, the model shows a good agreement for the near-field region when the measurement is taken at a distance halfway along the flame length (Zhou and Jiang 2016).
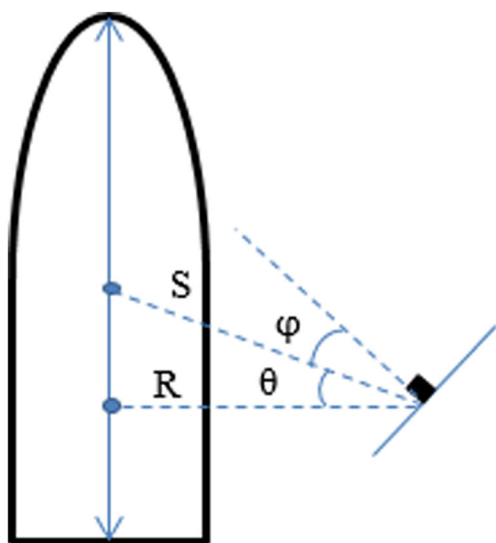
Figure 5 shows the schematic diagram of how the estimation is made using the MPSM model.

In order to determine the weight at each point, w_j, which is one of the parameters in MPSM, a correlation is proposed by Hankinson and Lowesmith (2012) as shown in Eq. (10):

$$w_j = \left[\begin{array}{l} w_j = jw_1 \\ n - \dfrac{n-1}{N-(n+1)}.(j-(n+1)) \\ \sum_1^N w_j = 1 \end{array} \right| w_1 \quad \begin{array}{l} j = 1,......,n \\ j = n+1,....,N \end{array} \right]$$

(10)

Hankinson and Lowesmith (2012) have established the applicability of weighted MPSM in the far-field radial distance up to 5 L. As can be seen in Fig. 6, as radial distance increases, and so is the normalized incident radiation. The value becomes close to unity at 2.5 L and 5 L of radial distance, indicating that the prediction of weighted MPSM is approximated to PSM when using distance, R. According to Zhou et al. (2016), PSM gives a good consistency on radiation measurement when the distance is more than twice the flame diameter in the horizontal direction.

In the case of near-field observation, it can be seen in Fig. 7a that the weighted MPSM and LSM show good consistency with the experimental data of Baillie et al. (1998) for small-scale jet fire in horizontal orientation, while for SFM using cylindrical shape as an assumption, the estimation gives the right trend for a radial distance more than 0.2 m. The underestimation of SFM in a radial distance less than 0.2 m may be due to incorrect flame shape assumption and this can be attributed to the buoyancy effects on the horizontal jet flame. In contrast, the simple MPSM overestimates the prediction. A possible explanation for the contrast might be
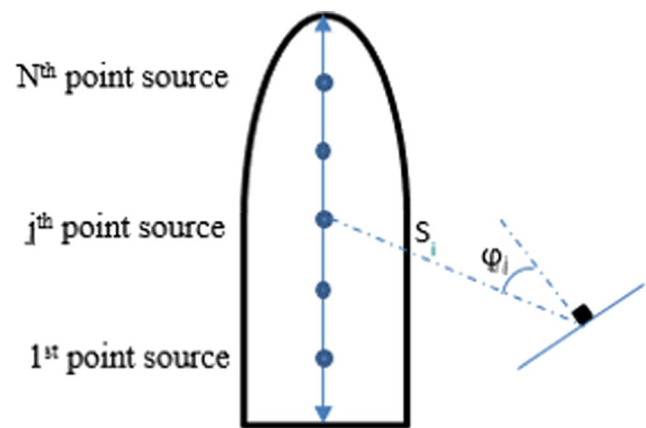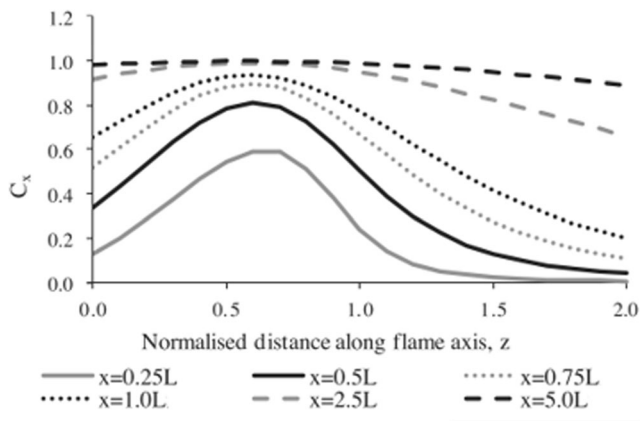

Fig. 4 Point source model with an inclined receiver

Fig. 5 Multipoint source model (MPSM) with the inclined receiver

Fig. 6 Normalized incident radiation ($C_x^{\text{MPSM/PSMR}}$) up to 5 L (Hankinson and Lowesmith 2012)

due to the weight of the distributed point along the jet flame centerline is assumed to be same in simple MPSM, while for weighted MPSM, the weight at each point is calculated as described by Eq. (10).
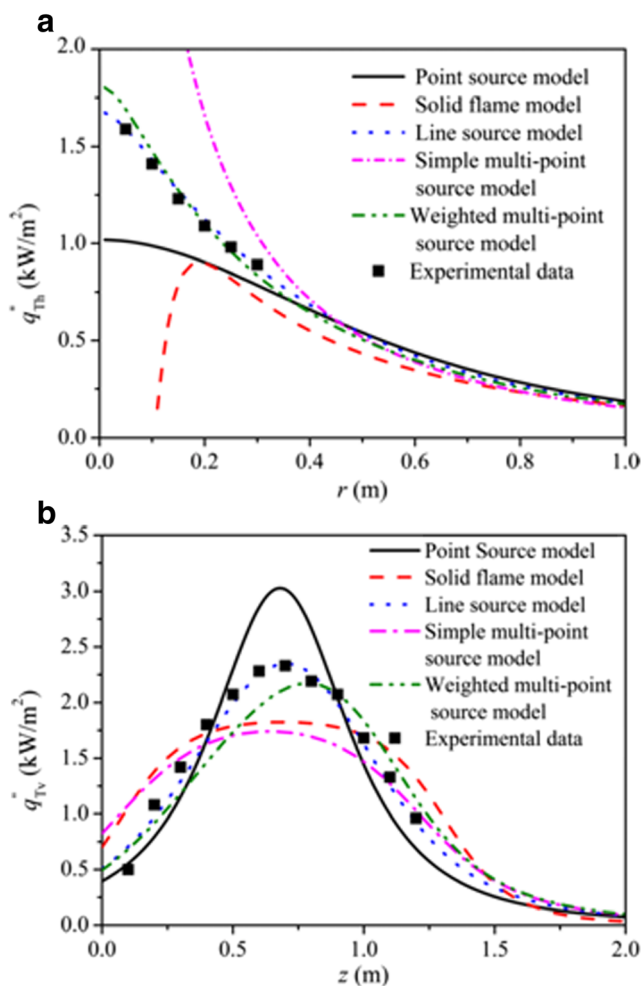
Fig. 7 Comparison of radiant heat profiles in the **a** horizontal direction and **b** vertical direction by different models (Zhou and Jiang 2016)

Flame Geometrical Features

Flame geometrical features are often used in radiant heat release prediction and possible impingement to the surrounding. Thus, it is very important to know the jet flame geometrical features. Flame geometrical features are usually determined through visual observation or photograph using visible flame emission (Becker and Liang 1978), infrared flame emission (Laboureur et al. 2016), or ultraviolet flame emission (Schefer et al. 2006). Geometrical features that best represent the jet flames should be carefully evaluated including the flame shape, length, width, and lift-off length to model the heat flux (Laboureur et al. 2016). The intensity of radiant heat release to the surrounding is directly proportional to release conditions that include release mass flow rate, release pressure, jet exit velocity, momentum, release diameter, and type of fuels. In SFM and LSM, the flame shape and its corresponding dimension are a function of the release condition factors, while in PSM and MPSM, the flame length and lift-off length are correlated with the release condition factors. It can be said that the factors are intercorrelated with each other, where at higher stagnant pressure and larger exit diameter, it will result in higher jet exit velocity, mass flow rate, and momentum (Palacios Rosas 2011). Eventually, it will produce longer jet flame, thus higher emissivity value and overall heat transfer to the surrounding. Flame geometrical features that will be discussed include the following:
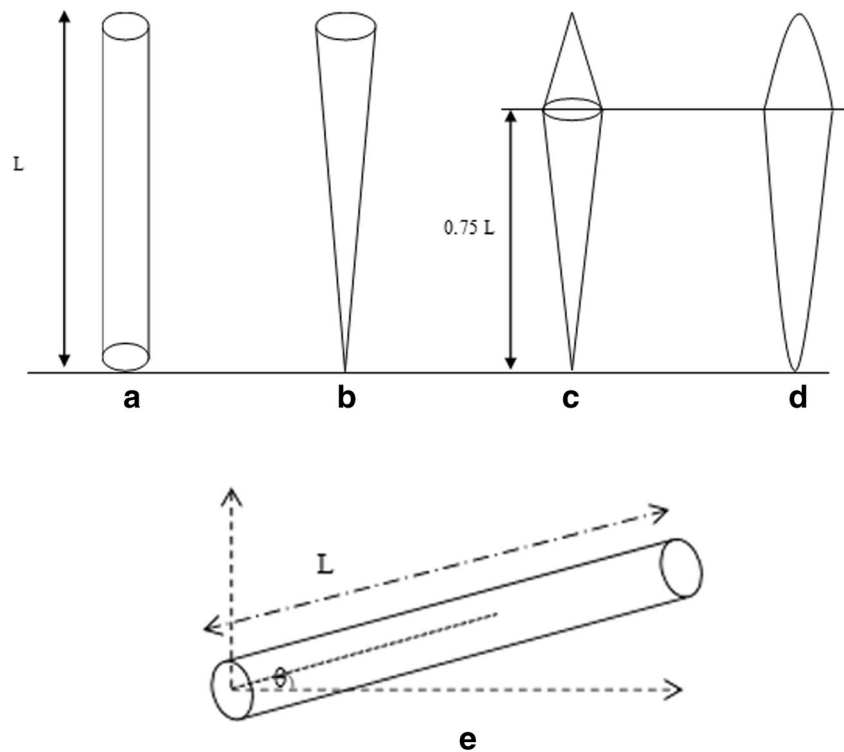
(i)   Flame shape
(ii) Flame length
(iii) Lift-off length
(iv) Flame width

Flame Shape

Assumption on jet fire flame shape is a common approach when using SFM and LSM predictions. The important aspect of the radiant heat transfer is the dimension and shape of the flame (Rajendram et al. 2015). Several shapes have been proposed in terms of release orientation. For vertical orientation, cylinder (Gómez-Mares et al. 2010; Hankinson and Lowesmith 2012; McCaffrey 1989), cone, back-to-back cone, back-to-back weighted ellipsoidal (Hankinson and Lowesmith 2012), and tilted cylinder (Rajendram et al. 2015) are among the flame shapes to describe the jet flame as given in Figs. 8 and 9. Cylinder, frustum of cone, ellipse, and kite flame shapes are favorable to the horizontal orientation as illustrated in Fig. 10 (Zhou et al. 2016; Zhang et al. 2015).

In general, the cylinder is often used as the flame shape for both horizontal and vertical orientations (Palacios and Casal 2011; Zhang et al. 2015; Palacios et al. 2012). For subsonic

Fig. 8 Shape configurations in solid flame model: **a** cylinder, **b** cone, **c** back-to-back cone, **d** back-to-back ellipsoidal, and **e** tilted cylinder

exit velocity, several flame shapes are proposed, i.e., elliptical and cylindrical. To the authors' knowledge, limited research was conducted to determine the flame shape at sonic exit velocity. Palacios Rosas (2011) in her study proposed that the radiating cylinder shape should be taken to represent the jet flame shape on vertical release into the quiescent environment at subsonic and sonic exit velocities. The radiating cylinder uses the radiant flame length L_{IR} as the flame length and the equivalent diameter D_{eq} is described as the flame width obtained from the 2D area (A_{IR}) of the jet fire surface determined by an algorithm developed in MATLAB through infrared image.

$$D_{eq} = A_{IR}/L_{IR} \tag{11}$$

In a study done by Laboureur et al. (2016), they recommended that rectangle and kite shapes best represented the horizontal flame shape for radiation measurement. An earlier study by Sonju and Hustad (1984) on turbulent propane and methane jet flame found that emissivity E increases linearly with respect to flame length and has a good agreement with the work carried out by Kozanoglu et al. (2011) on convection heat transfer. It is commonly assumed that the E value is constant over the entire flame surface. However, the assumption of an ideal flame shape may not truly represent the real flame area, and thus, the true value of emissive power E might deviate from the real value. Furthermore, the assumption made could give an error in estimating the thermal radiation intensity in the case of near-field smoke-producing hydrocarbon

fires. Although the interpretation of flame shape is varied among studies when the SFM is applied, the applicability is still valid and widely used in many industrial calculations. The application of SFM is not only restricted to jet fire but to another type of fires such as a pool fire.

Zhou and Jiang (2016) proposed the modification for E based on flame length instead of flame area due to inconsistent result on thermal radiation intensity, known as emissive power per line length (EPPLL). The suggested flame shape for vertical and horizontal orientations can be seen in Figs. 9 and 10, respectively. In this context, radiant heat is assumed to be emanated from the centerline inside the jet flame volume. Thus, the resulted data is the EPPLL (kW m^{-1}) as compared to per flame area (kW m^{-2}) as described in the SFM, and the deviation can be reduced as much closer to the true emissivity value when using LSM for radiant heat estimation.

Based on a study conducted by Zhou and Jiang (2016), the most suitable shape to represent the small-scale vertical jet fire is back-to-back cone shape, while for bigger vertical jet release flame with a length at approximately 10 m, a combined shape of a cylinder on the upper side and of a cone on the lower site was found to be most suitable. They also found that the kite shape flame was the best fit for radiant heat estimation for medium-scale horizontal jet fire. In addition, lift-off length must be considered once using LSM for thermal radiation calculation particularly in near-field observation.

As can be seen in Fig. 11, the inclusion of lift-off holds considerable effects on the radiant heat release.
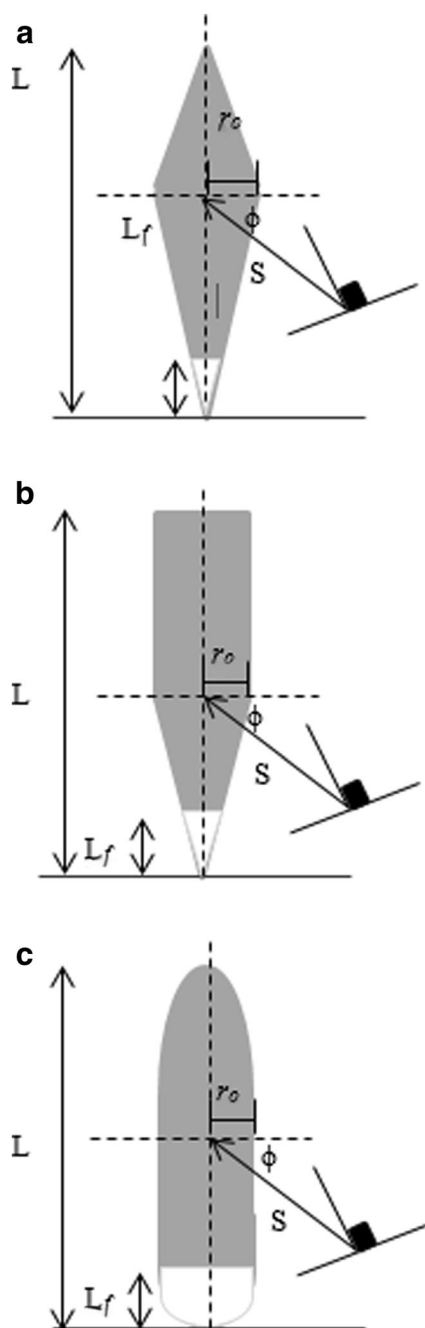
Fig. 9 Shape combinations in the vertical line source model: **a** cone–cone, **b** cylinder–cone, and **c** ellipse–ellipse

However, all assumptions made are only applicable to the perfectly horizontal-oriented jet flame. In reality, the flame shape tends to deform on horizontal jet fire due to buoyancy effects (Ekoto et al. (2014), and this condition gives underpredicted value of the fraction of heat radiated by 40% or more. The increasing optical path length between the sensor and the flame centerline is in the buoyancy-dominated region, and this condition causing the radiant heat release was not fully captured. The flame shape deformation will certainly

affect the flame length correlation, and this will be discussed further in the next section. It can be summarized that flame shape is one of the important features in SFM and LSM radiant heat prediction. It gives a direct effect on the emissivity value per area (kW m^{-2}) when using SFM and on the emissivity value per line length (kW m^{-1}) when LSM is applied.
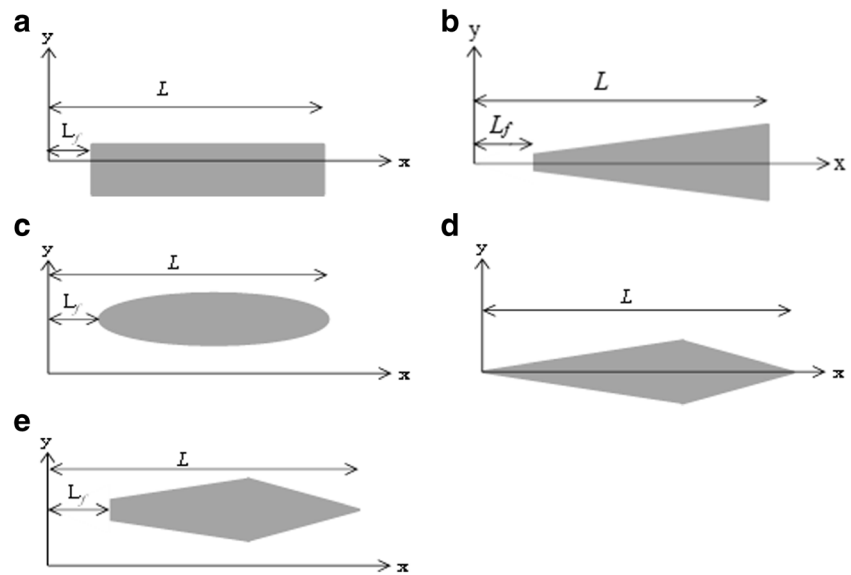
Flame Length

Flame length (L) is defined as the distance between the nozzle exit to the farthest flame tip and usually controlled by the mixing process of air and fuel release (Gopalaswami et al. 2016). It is one of the important geometrical features of jet flame. The flame length estimation method has evolved over time where there is no definitive method on the number of images taken or time interval. In earlier predictions of flame length, there are two common methods used: (i) models based on stoichiometric and momentum considerations and (ii) correlations based on fuel or momentum flow that takes into account the effect of buoyancy, generally of an empirical nature (Bagster and Schubacht 1996).

As technology advances, from using manual method of visual observation, to processing using software, the number of images used to estimate flame length always varies: 30 images (Røkke et al. 1994), 90 images (Sugawa and Sakai 1996), and 30–50 images or within 10 s time interval (Lowesmith and Hankinson 2013). Flame length is used to indicate the emissive power, EPPLL in LSM, and to locate the source emitter in PSM and MPSM. In PSM and MPSM, the location of a point source in which the radiant heat is emanating lies within the axis of the flame length. It is assumed that the point should be at the center for PSM and evenly distributed along the flame axis for MPSM. There are two types of MPSM that are commonly employed: simple MPSM where the weight of source points within the flame axis is similar throughout the line and weighted MPSM in which the weight can be predicted using Eq. (10) which lies within the central line axis. Hankinson and Lowesmith (2012) observed that the weighted MPSM was capable of deriving near-field and far-field radiation as compared to PSM, in which the prediction is only satisfactory for far field only.

In order to obtain the jet flame length, there are several guidelines in which the flame length is varied according to numerous factors such as fuel velocity, leak size, mass flow rate, material release density, stagnation pressure, and net heat released. An earlier study to predict flame length suggested that flame length is independent to velocity increment or may vary slightly with velocity (Hawthorne et al. 1949). However, later findings have found that flame length was a function of mass flow rate (Wertenbach 1971; Schefer et al. 2004; Palacios et al. 2009; Mogi and Horiguchi 2009; Kalghatgi 2010).

Fig. 10 Shape configurations in the horizontal line source model: **a** cylinder, **b** frustum of cone, **c** ellipse, **d** kite (ignoring lift-off), and **e** kite (including lift-off) (Zhou et al. 2016)

Palacios and Casal (2011) found in their study that flame length is based on heat released by combustion, stagnation pressure, outlet orifice diameter for subsonic jet flow, and fictitious diameter of the sonic jet flow. In addition, different characterizations of flame length have been proposed based on the dimensionless number of Froude (Gopalaswami et al. 2016), Richardson (Becker and Liang 1978; Kalghatgi 2010), and Reynolds (Palacios and Casal 2011). A summary of experimental works and suggested correlations for flame length as a function of mass flow rate, Reynolds number, and Froude number is presented in Table 2.

As can be seen in Fig. 12, the correlation developed by Zhou et al. (2016) can fit the horizontal jet release data of experiments (Smith et al. 2005; Zhang et al. 2015; Gopalaswami et al. 2016; Tao et al. 2016), while the correlation by Suris et al. (1978) shows a higher coefficient, indicating that the correlation for vertical jet fire may not be

Fig. 11 The lift-off effect on kite shape assumption: predicted value versus experimental measurement (Zhou et al. 2016)

applicable to horizontal jet fire. Furthermore, the applicability of flame length correlations based on Froude number is more suitable for subsonic jet release (Palacios Rosas 2011). Later findings by Schefer et al. (2006) gave an opposite observation, as they verified that the correlation is also valid for the underexpanded or sonic jet release. Another correlation was proposed as a function of jet exit diameter in the momentum-dominated regime as
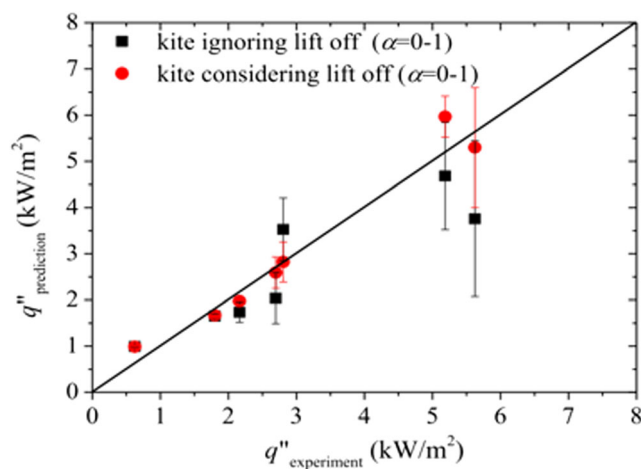
$$L = 23(d/f_s)(\rho_s/\rho_\infty)^{1/2} \tag{12}$$

where L, d, f_s, ρ_s, and ρ_∞ are the visible flame length, the jet exit diameter, the mass fraction of fuel at the stoichiometric condition, the gas density at the jet exit, and the ambient gas density, respectively. From their study, it can be deduced that the higher diameter of the nozzle exit results in higher flame length. Work done by Molina et al. (2007) gave a similar observation for flame length where the value is proportional to total jet mass flow rate and jet exit diameter.

Another correlation was proposed based on orifice's Reynolds number based on a claim made by Palacios et al. (2009) that the value can be used for both subsonic and sonic regimes as shown in Table 2. A study by Mogi and Horiguchi (2009) suggested the correlation of the flame length as a function of stagnation pressure on their work of horizontal hydrogen jet diffusion flame at nozzle in the range of 0.1 to 4 mm from a storage pressure range of 0.01 to 40 MPa. The proposed correlation is as follows:

$$L/d = 530P_0^{0.43} \tag{13}$$

where L, d, and P_0 are the flame length, nozzle diameter, and stagnation pressure, respectively. The correlation proposed is

Table 2 Experimental works of flame length correlation as a function of various parameters, namely, mass flow rate, m; Froude number, Fr; and Reynolds number, Re

Reference	Jet orientation	Fuel	Nozzle size (mm)	Fr/Re range	Correlation
Wertenbach (1971)	–	–	–	–	$L = 18.5m^{0.41}$
Sonju and Hustad (1984)	Vertical	Propane	2–80	80 to 6.10^5	$L/d = 27Fr^{0.2}$
		Methane		5.10^2 to 1.10^5	$L/d = 21Fr^{0.2}$
McCaffrey (1989)	Vertical	Methane	≤ 30	Up to 1.10^5	$L/d = 28Fr^{0.2}$
Santos and Costa (2005)	Vertical	Propane	5–8	315–46,407	$L/d = 36Fr^{0.2}$
		Ethylene		7870–384,791	$L/d = 24Fr^{0.2}$
Palacios et al. (2009)	Vertical	Propane	10–43	Up to 1.10^6	$L/d = 61Fr^{0.11}$
	Vertical	Propane	10–43	Up to 1.10^7	$L/d = 58Re^{0.27}$
Palacios and Casal (2011)	Vertical	Propane	10–43	Up to 1.10^7	$L/d = Re^{0.4}$
Gopalaswami et al. (2016)	Horizontal	Propane	19	2.10^3 to 23.10^5	$L/d = 23Fr^{0.2}$
Tao et al. (2016)	Horizontal	LPG	8, 12, 16	Up to 1.10^3	$L/d = 25.6Fr^{0.2}$
Zhou et al. (2016)	Horizontal	Propane	1.5–19.1	Up to 1.10^5	$L/d = 22Fr^{0.2}$

somewhat overestimated for flame length prediction, as reported by Studer et al. (2009) for horizontal pure hydrogen and hydrogen/methane jet release from the orifice diameter of 4, 7, and 10 mm. The proposed correlation obtained in their study is

$$L/d = 420P_0^{0.43} \tag{14}$$

Besides, the flame height is higher at lower atmospheric pressure as concluded by Hu et al. (2013a) when the work was carried out in a reduced atmosphere at two different altitudes—50 m (100 kPa) and 3650 m (64 kPa). For flame length, the prediction is based on heat release rate. A study for
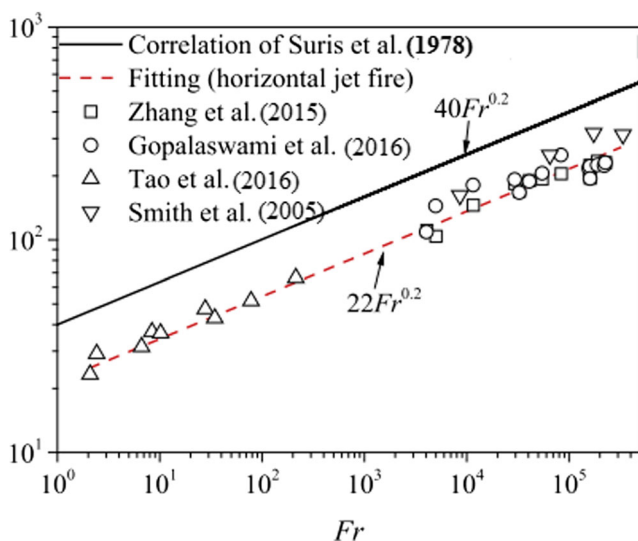

Fig. 12 Flame length correlation with a range of Froude number (Zhou et al. 2016)

buoyancy-controlled liquefied petroleum gas (LPG) turbulent jet diffusion flame from the inclined nozzle (0°, 30°, 45°, 60°, and 90°) (Tao et al. 2016) resulted in the following expression:

$$L/d = \left(Q_s^*\right)^{2/5} c_2 \tag{15}$$

where L, d, Q_s^*, and c_2 are the flame length, nozzle diameter, dimensionless heat release rate, and constant parameter, respectively. From their study, the rate of air entrainment is proportionally inversed to the angle increment, in which lesser heat releases to the ambient when the nozzle is fully inclined to 90° (Tao et al. 2016). Thus, it implies that a higher inclination angle leads to shorter flame length, at a fixed nozzle diameter.

The previous correlation in Table 2 and Eqs. (12)–(14) was developed based on the assumption that the trajectory of the jet flame is linear; however, in real cases, the flame shape deformation would cause underprediction of radiant heat release. Ekoto et al. (2014) performed two large-scale flame experiments, using hydrogen as fuel source released from the circular nozzle with a diameter of 20.9 and 52.5 mm. The suggested method to optimize the heat source emitter in flame centerline trajectories is by employing a new developed 1D flame integral model where the mass, momentum, and mixture fraction were integrated over the flame cross-sectional area and differentiated along the flame centerline as clearly illustrated in Fig. 13.

In the case where the flame resulted is at a lower flow rate or small scale, the projection distance (L_p) is defined as the horizontal distance from the nozzle exit to the farthest point of the flame as shown in Fig. 14.

Fig. 13 Schematic of the 1D buoyant jet flame model (Ekoto et al. 2014)

Discharge point

Flame centreline   Flame cross sectional area
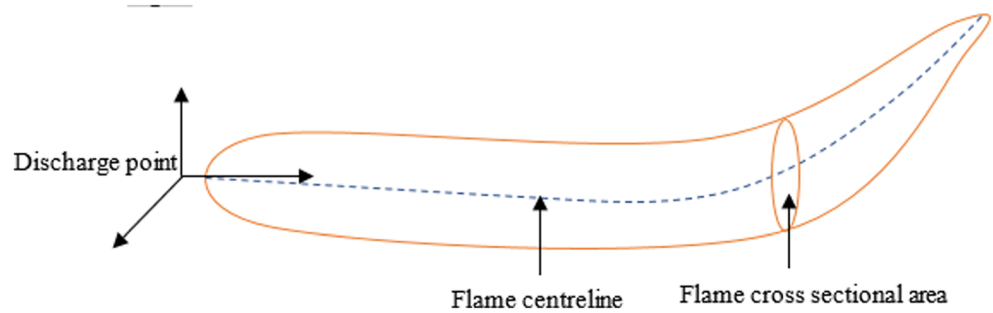
A general correlation developed is applicable for jet release from nonaxisymmetric and axisymmetric rectangular nozzles of different aspect ratios (AR = L_n/W_n) that vary from 1–1 to 71–1 where L_n is the nozzle length and W_n is the nozzle width. In this study, propane was used as fuel (Zhang et al. 2017).

$$\frac{L_p}{W_n} = 0.376(\Pi)^{2/3}, \quad 83 < \Pi < 7794 \tag{16}$$

$$\frac{L_p}{W_n} = 4.102(\Pi)^{2/5}, \quad 7794 < \Pi < 1.61 \times 10^7 \tag{17}$$

where Π is the nondimensional variable defined as:

$$\Pi = \left(\frac{T_\infty}{\Delta T_{f,a}}\right)^{3/4}\left(1 + \frac{T_\infty}{\Delta T_{f,a}}\right)^{3/4}Q^*_{\zeta_1} \tag{18}$$

$$Q^*_{\zeta_1} = \frac{Q}{c_p\rho_\infty T_\infty\sqrt{g}\left(W_n^{7/10}L_n^{3/10}\right)^{5/2}} \tag{19}$$

While most of the correlation developed is valid for hydrocarbon jet flame and not particularly effective for low luminosity gases such as hydrogen and syngas mixture, Miller (2017) developed a method to determine the flame length in both horizontal and vertical orientations. The method to determine overall centerline flame length is similar to Ekoto et al. (2014), where both the momentum and buoyancy region are taken into account. The flame length in the momentum region is designated as L_m, flame length in the buoyancy region is designated as L_b, and flame length with zero wind is designated as L_0. The schematic diagram of jet release which accounts for buoyancy effects can be seen in Fig. 15.

The equation used for vertical jet flame is adopted from Chamberlain (1987):
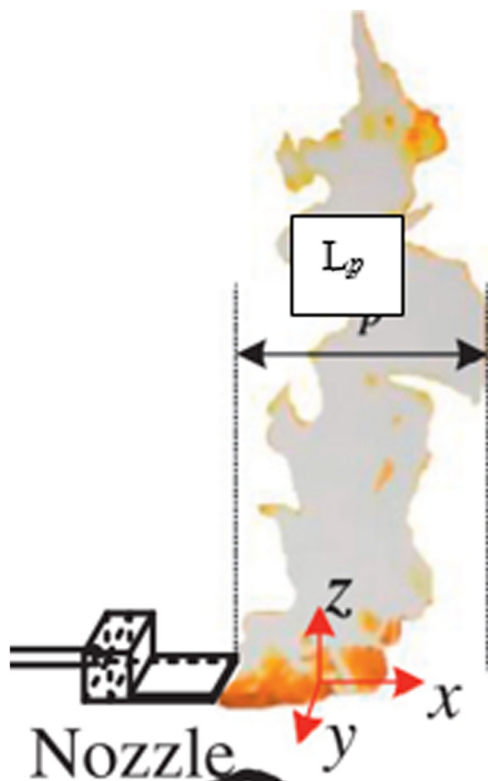
Fig. 14 Flame projection distance L_p (Zhang et al. 2017)
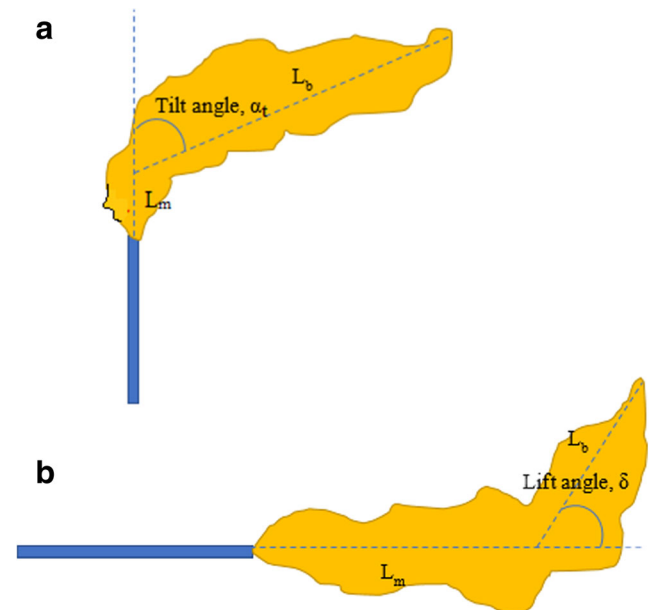
Fig. 15 Flame geometry with buoyancy effects in **a** vertical orientation and **b** horizontal orientation (Miller 2017)

$$L_m = \begin{cases} 0.2L_0, & \text{for } \alpha=0 \\ L_0\dfrac{\sin(K\alpha)}{\sin(\alpha)} & \text{for } \alpha\neq0,\ \alpha\neq\pi \ K=0.185e+0.015 \\ 0.015L_0 & \text{for } \alpha=\pi \end{cases}$$

$$(20)$$
$$(21)$$
$$(22)$$

$$L_b = \left(L_0{}^2 - L_m\sin(\alpha)\right)^2\right)^{0.5} - L_m\cos(\alpha) \tag{23}$$

The equation used for horizontal jet flame is

$$\frac{L_m}{L_0} = -0.125\xi(L_0) + 1.25 \quad 0\leq\frac{L_m}{L_0}\leq1 \tag{24}$$

$$L_b = \left(L_0{}^2 - L_m\sin(\delta)\right)^2\right)^{0.5} - L_m\cos(\delta) \tag{25}$$

The overall flame length L in both orientations is

$$L = L_m + L_b \tag{26}$$

Due to the aforementioned finding of underprediction of radiant heat release due to buoyancy effects, it is therefore suggested that the buoyancy effects should be taken into consideration on the imperfect trajectory of horizontal jet fire in order to obtain a good estimation of flame length.

Lift-Off Length

Lift-off length (L_f) is another significant characteristic of jet flame as it affects the overall flame length and formation of soot which further determines the amount of heat released to the surrounding (Palacios Rosas 2011), flame stabilization (Wang et al. 2014), turbulence–chemistry interaction, and local extinction (Lyons 2007). Flame lift-off was defined as the separation distance of the visible flame and jet exit (Kalghatgi 1983; Bradley et al. 2016). A recent study by Zhou and Jiang (2016) using LSM stated that the inclusion of lift-off to determine the flame length could give variation in the total radiant heat release. From their study, it was observed that the horizontal release orientation gives a higher lift-off value than the vertical release (Zhou et al. 2016). This is due to the gravitational effect and viscous friction on the vertical orientation jet fire. The work implies that the flame length that includes the lift-off length may give a good estimation of radiant heat release as compared to that when the lift-off flame is excluded in the estimation. This study contradicts with the assumption made by Gómez-Mares et al. (2010) and Palacios et al. (2012) when using SFM in which the flame length is determined at the visible bottom to the top of the flame, excluding the lift-off. On the other hand, determination of point source in PSM and MPSM is based on the flame length that includes the lift-off length. Although many correlations include the lift-off distance as a function of velocity and burner exit diameter as listed in Table 3, one should be careful to reapply the correlations by taking into account the jet flame direction at first.

Table 3 Experimental work on lift-off length

References	Jet orientation	Fuel type	Nozzle size (mm)	Fr range	Correlation
Peter and Williams (1983)	Vertical	Methane	4–12	–	$L_f/d = 3.6 \times 10^{-3}(u/d)$
McCaffrey (1989)	Vertical	Methane	≤30	Up to 1.10^5	$L_f/d = 0.05Fr^{0.5}$
Santos and Costa (2005)	Vertical	Propane	5–8	315–46,407	$L_f/d = 2.6 \times 10^{-3}(u/d)$
		Ethylene		7870–384,791	$L_f/d = 0.8 \times 10^{-3}(u/d)$
Kiran and Mishra (2007)	Vertical	LPG	2.2	Up to 1.10^5	$L_f/d = 1.8 \times 10^{-3}(u/d)$
Palacios et al. (2009)	Vertical	Propane	10–43	Up to 1.10^6	$L_f/d = 0.62Fr^{0.3}$
					$L_f = 6 \times 10^{-4}Re^{0.5}$
Wang et al. (2014)	Vertical	Propane	4, 5, 6	–	60 kPa; $L_f = 0.00564u - 0.000253$
					70 kPa; $L_f = 0.00473u - 0.001381$
					80 kPa; $L_f = 0.00438u - 0.03438$
					90 kPa; $L_f = 0.00385u - 0.03288$
					100 kPa; $L_f = 0.00255u - 0.01602$
Gopalaswami et al. (2016)	Horizontal	Propane	19	2.10^3 to $2.3.10^5$	$L_f/d = 9.7 \times 10^{-3}(u/d)$
Zhou and Jiang (2016)	Vertical	Methane	8.6	69	$L_f/d = 3.6 \times 10^{-3}(u/d)$
Zhou et al. (2016)	Horizontal	Propane	–	Up to 1.10^5	$L_f/d = 9.55 \times 10^{-3}(u/d)$

A previous study indicated that different burner diameters do not give a significant variation for flame lift-off; however, the value increases linearly with jet exit velocity (Kalghatgi 1983). As the jet velocity increases, more air will be entrained, and this could enhance the combustion process, by producing more premixed blue flame, leading to lifted flame. However, as stable flame length is reached, lift-off length will become increasingly sensitive to air entrainment (Kalghatgi 1983). The correlation proposed by Kalghatgi (1983) on this phenomena is as follows:

$$L_f = 0.141(G\rho_\infty)^{0.5} \tag{27}$$

$$G = \pi\rho_j u_j^2 d \tag{28}$$

where G, ρ_j, U_j, and d_j are the initial jet momentum flux, expanded jet density (kg m^{-3}), expanded jet velocity (m/s), and expanded jet diameter (mm), respectively. A similar correlation has been applied to a work involving LPG horizontal jet fire issuing through 19 mm diameter nozzle at a velocity range of 25 to 210 m/s (Gopalaswami et al. 2016). Yet, this work gave an overprediction of lift-off length as compared to other previous studies using the same model (Suris et al. 1978; Sonju and Hustad 1984; Johnson et al. 1994; Santos and Costa 2005; Kiran and Mishra 2007; Palacios et al. 2009). It can be suggested that the lift-off length is highly sensitive to the threshold parameter in image processing analysis. Nonetheless, the dimensionless correlation was proposed based on the experimental dataset as

$$L_f/d = 9.7 \times 10^{-3}(u/d) \tag{29}$$

which is based on the primary equation that was first developed by Peter and Williams (1983) as per Eq. (30) when c is constant with a dimension of time (s)

$$L_f/d = c(u/d) \tag{30}$$

However, Hu et al. (2013a) observed that the lift-off height is increased when the velocity increases on propane jet diffusion flame at a reduced atmosphere. From their work, the correlation at 64 and 100 kPa, respectively, has been developed

$$\text{At 64 kPa,} \quad L_f/d = 1.36u - 5.88 \tag{31}$$

$$\text{At 100 kPa,} \quad L_f/d = 0.6u - 5.33 \tag{32}$$

The result was in good agreement with the study done on vertical diffusion jet flame using propane as sample fuel from a circular nozzle between 4 and 6 mm diameter at the subatmospheric conditions of 60, 70, 80, and 90 kPa and normal atmospheric condition of 100 kPa (Wang et al. 2014). Palacios et al. (2016) observed in their work, for subsonic jet flame, a

normalized lift-off distance which can be defined as

$$(L_f/d)f = 0.1U^* - 0.2 \tag{33}$$

The data gathered by Bradley et al. (2016) has deduced the following equations for subsonic and sonic flame:

$$(L_f/d)f = 0.11U^* - 0.2 \quad \text{in the subsonic regime} \tag{34}$$

$$(L_f/d)f^{0.2} = -54 + 17\ln(U^* - 23) \text{ in the chocked and} \tag{35}$$
$$\text{supersonic regime}$$

where f is the ratio of fuel to air moles in fuel–air mixture for maximum burning velocity and U^* is the dimensionless flow number expressed as

$$U^* = (u/S_L)(d/\delta)^{-0.4}(P_i/P_a) \tag{36}$$

where u, S_L, d, δ, P_i, and P_a are the velocity (m/s), maximum laminar burning velocity of the mixture under ambient conditions (m/s), nozzle diameter, laminar flame thickness under ambient conditions (m), initial pressure, and ambient pressure, respectively. In the vertical direction, the lift-off may give a constant value at a point as the velocity increases. It can be explained by the gravitational force and a similar observation should be applied for horizontal orientation. Besides, the lift-off is dependent on the fuel type, by introducing the multiplying factor f as in Eqs. (33)–(35). From the discussion above, a summary of lift-off length correlation based on velocity, Froude number, and Reynolds number is summarized in Table 3.

Flame Width

In the literature, determination of radiant heat release was said to be closely related to flame length, shape, and lift-off length. There is a little attention given to the flame width which is directly linked to the flame shape configuration. It can be said that the flame width (W_0) is proportional to flame length and approximately equal to $0.18 L$ (Mogi and Horiguchi 2009) for sonic hydrogen jet release in a horizontal orientation. Palacios and Casal (2011) investigated flame width from propane jet release in a vertical orientation at a different location along the flame length. It was found that flame width gives a better prediction at point of $0.7 L$ for both sonic and subsonic releases. Although flame width data are not usually included in the semi-empirical model, however, as an improvement made in LSM, the determination of flame width is equally important to flame length, shape, and lift-off. It was used to determine the average flame radius for flame emissivity calculation (Zhou and Jiang 2016; Zhou et al. 2016) and, consequently, the total amount of radiant heat released to the surrounding. In

the case of flame impingement, the flame width may have a direct impact on the localized heat flux area. Since it was a function of velocity, thus, it can be said that the impinged area should be larger when jet release velocity is increasing.

Total Heat Release and Radiative Fraction

Other key parameters to be considered for radiant heat prediction are the total heat release and radiative fraction. It is especially important in PSM and MPSM models. Total power of combustion Q_T is a direct function of mass flow rate m (kg s^{-1}) and net calorific value of the fuel H (kJ kg^{-1}).

$$Q_T = mH \tag{37}$$

Radiative fraction η is defined as the ratio of total radiant heat emitted Q_R by the jet flame to the total heat release rate Q_T (Zhou et al. 2018). It is also defined as the amount of flame energy converted into escaping radiant energy. A normal way to obtain the η data is through experimental measurement for both Q_R and Q_T of the jet release.

$$\eta = \frac{Q_R}{Q_T} \tag{38}$$

The determination of the radiative fraction η is based on several factors such as fuel type, atmospheric condition, fuel flow rate, distance of measurement (near field and far field), geometry of fire, and fuel release conditions (velocity, temperature, and orientation) (Hankinson and Lowesmith 2012; Miller 2017). The applicability of η cannot simply be assumed. For example, if the η value is determined using the PSM model, similar η value should not be applied if one adopts the MPSM model in their heat release prediction. The situation is also applied to near- and far-field observations where η is determined in the far field from a jet fire, limiting the applicability to near-field observation (Hankinson and Lowesmith 2012).

An earlier study by Chamberlain (1987) correlates the radiative fraction with orifice exit velocity using natural gas as fuel in a vertical orientation.

$$\eta = 0.21e^{-0.00323u_{eq}} + 0.11 \tag{39}$$

where u_{eq} is the effective exit gas velocity of the gas jet given by Birch et al. (1984)

$$u_{eq} = u_j + \left(p_j - p_\infty\right) / \left(\rho_j u_j\right) \tag{40}$$

where p_j and p_∞ are the absolute pressures at the jet exit pressure and in the atmosphere, respectively, while ρ_j is the jet exit density. Release flow from the jet exit forms an underexpanded jet and rapidly expands to ambient condition through a series of expansion shock (Schefer et al. 2006). The

concept of the underexpanded jet is also known as a notional nozzle that has been explored by others (Birch et al. 1984; Schefer et al. 2006; Molina et al. 2007; Ekoto et al. 2014) as shown in Fig. 16. Effective diameter d_{eff} is introduced in this concept, on the basis of mass and momentum conservation equation (Molina et al. 2007), in which the value is often larger than the nozzle diameter.

From Fig. 16, level 1 indicates a high-pressure source (P_1) with a temperature of (T_1); level 2 is the jet exit with release diameter, pressure, temperature, and velocity of (d_2, P_2, T_2, v_2), while level 3 is the ambient condition where the jet expands to temperature, pressure, and velocity of (T_2, P_2, v_2). It is assumed that the velocity is uniform at level 3 and usually at sonic condition. Another assumption is made which includes that there is no air entrainment between levels 2 and 3 (Molkov and Saffers 2013). The diameter of d_{eff} is usually larger than the jet exit diameter, d_2. In this particular case, the η value drops with the increase of jet velocity due to improved combustion quality with the lower portion of the jet beginning to become blue at larger jet velocity (Kiran and Mishra 2007; Zhou and Jiang 2016).

Markstein and Ris (1990) have carried out experiments on the radiative fraction against total heat release and correlated radiative fraction to global residence time, derived from a convective timescale. Molina et al. (2007) coupled global residence time to correction factor; however, the application is limited to nonsooting flame such as hydrogen in the momentum-controlled regime. Radiative fraction value is dependent on the fuel type and its reactivity, which will determine the combustion quality. The combustion quality and its associated heat release can be correlated to its carbon content and type of bonds, i.e., alkanes, alkenes, and alkynes. There are numerous studies that have been conducted to compare the combustion quality and fraction of heat radiated by different types of carbon number (Lowesmith et al. 2007). The fuels include butane, propane, natural gas, crude oil, and butane/ natural gas mixtures. For hydrocarbon with higher carbon content, more soot is produced with higher emission and, thus,
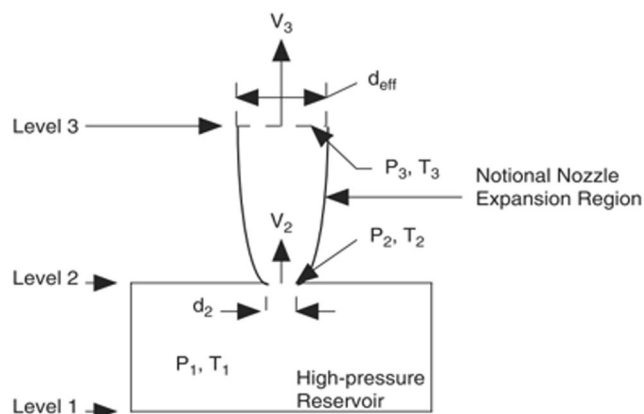
Fig. 16 Notional nozzle concept (Birch et al. 1984)

induced more heat radiated (American Petroleum Institute 2008). From the work of Hankinson et al. (2007), they suggested that the radiative fraction was 0.13 for natural gas, 0.24 for propane, 0.32 for butane, and 0.5 for crude oil. For the mixtures of butane/natural gas, the radiative fraction is directly proportionated with butane content; when the content of butane in mixtures increases, the fraction of heat-radiated η would also increase.

The work of Lowesmith and Hankinson (2012) reported that fuel mixtures are dependent on the carbon content of the individual component that contributes to the highest percentage of total mass. For liquid–gas mixtures, η can be estimated by using the following equation as proposed by Lowesmith et al. (2007):

$$\eta_m = \left(\frac{x}{100}\right)(\eta_L - \eta_G) + \eta_G \qquad (41)$$

where η_m is the fraction of heat radiated of the mixture, x is the mass percentage, η_L is the fraction of heat radiated of liquid, and η_G is the fraction of heat radiated of gas. Studer et al. (2009) have conducted a study of large-scale methane/hydrogen jet fire and found that when the methane content (%) increases in the mixture, the fraction of heat radiated would also increase as depicted in Fig. 17.

Based on the work reported by Lowesmith et al. (2007) on the fraction of heat radiated and the relation to field of observation, it can be said that PSM is not suitable to be used at a near distance (within one flame length) and this gives an advantage for SFM to be adopted on heat release prediction. If one used PSM for measurement of incident radiation data in the near field, the correction factor is needed to apply in order to obtain the correct fraction of heat radiated or otherwise use the weighed MPSM approach. The effects of near field and far field on the fraction of heat-radiated measurement have been extensively explored by Hankinson and Lowesmith (2012) using various modeling approaches that include SFM, PSM, and MPSM. From their findings, the PSM approach may provide erroneous results for a radiative fraction if incident radiation data (Q_R) in the near field is used. Meanwhile, the use of MPSM shows better agreement with near-field observation. Figure 18a–f shows the prediction models in near-field observation as a function of normalized distance along the flame axis and the comparison between the experimental data from Sivathanu and Gore (1993) and Baillie et al. (1998). From the figures, it can be seen that the normalized incident radiation ($C_x = Q^{meas}/Q^{model}$) of selected models is based on the single-point source model using distance R (refer to Fig. 4), called PSMR.

Figure 18a shows the prediction value of C_x at a radial distance of 0.5 L and varying axial location using Q^{meas} of MPSM, Fig. 18b using Q^{meas} of PSM with distance S, Fig. 18c using Q^{meas} of SFM with cylinder shape, Fig. 18d using Q^{meas} of SFM with cone shape, Fig. 18e using Q^{meas} of SFM with back-to-back cone shape, and Fig. 18f using Q^{meas} of SFM with back-to-back ellipsoid.

It can be clearly seen on Fig. 18a that the predicted value of $C_x^{MPSM/PSMR}$ peak is in the correct region in the axial direction and the curve lies within the bounds of the data presented by Sivathanu and Gore (1993), while Fig. 18b shows the overpredicted value of C_x and the peak obtained was slightly off to the left when compared with the experimental data values, implying poor agreement with the data when using PSM prediction. Figure 18c use an assumption of cylindrical shape when prediction using SFM is adopted, and it shows an overpredicted value and earlier peak detected at lower radial distance. SFM with conical shape shows slightly better agreement than when the cylinder shape is used as illustrated in Fig. 18d. In Fig. 18e–f, when using SFM with back-to-back cone and ellipsoidal shape, respectively, it shows agreeable data in terms of shape and peak location. From the comprehensive comparison between model prediction and experimental data, it can be concluded that MPSM offers a better approach for radiant heat prediction in the near field, and PSM is unsuitable for near-field observation, while SFM is suitable

Fig. 17 Fraction of heat radiated for fuel mixtures (Hankinson et al. 2007)
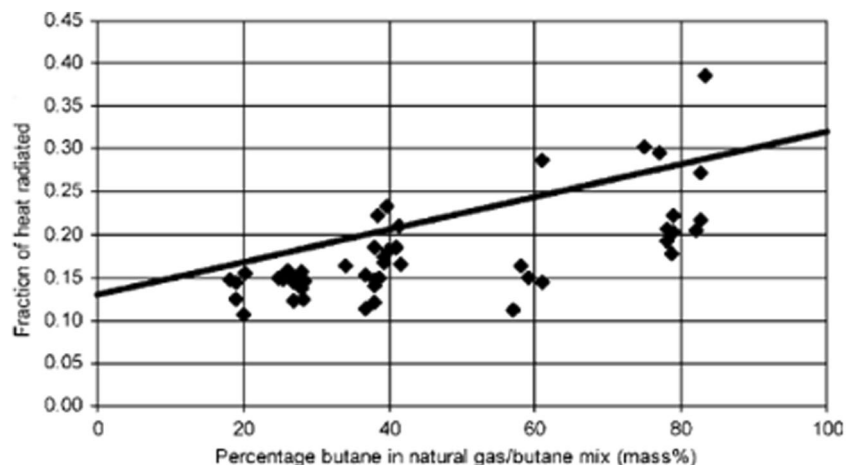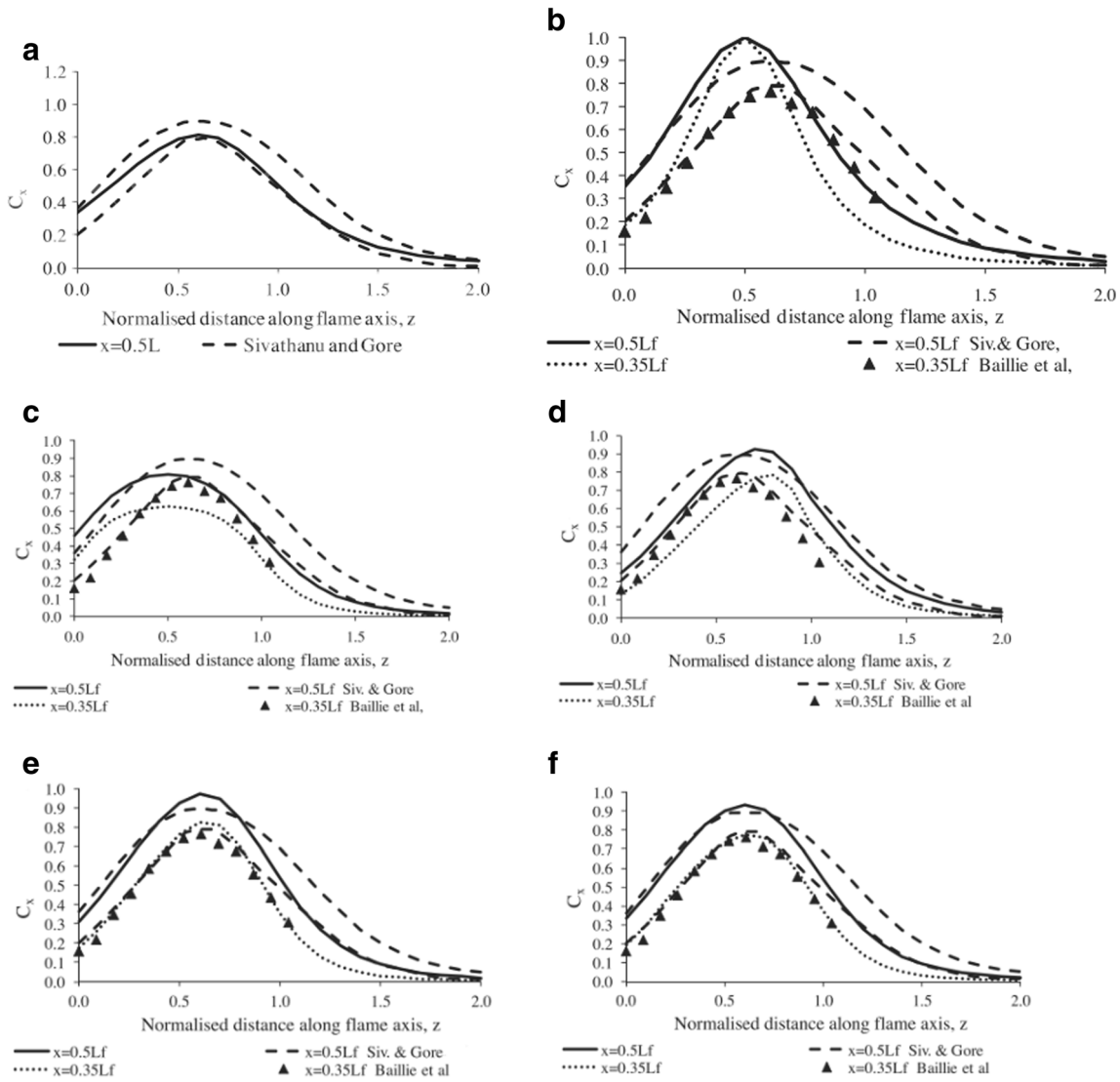
Fig. 18 Prediction of normalized incident radiation (C_x) vs. experimental data of Sivathanu and Gore (1993) and Baillie et al. (1998): **a** $C_x^{MPSM/PSMR}$, **b** $C_x^{PSMS/PSMR}$, **c** $C_x^{CYL/PSMR}$, **d** $C_x^{CON/PSMR}$, **e** $C_x^{BBC/PSMR}$, and **f** $C_x^{BBE/PSMR}$ (Hankinson and Lowesmith 2012)

if the correct flame shape is used to represent the flame configuration.

Other than that, jet fire orientation also holds considerable effects on the radiative fraction as indicated by Zhou et al. (2016). In their study, they have correlated Froude number to radiant heat fraction. However, there is no physical interpretation in detail.

In general, most of the correlations for radiative fraction are not valid to low luminosity gases such as hydrogen and syngas mixtures (Miller 2017). Thus, a series of experiments have been conducted using hydrogen and syngas as fuel in a vertical and horizontal orientation. The model developed in the study called AP flame adopted the MPSM approach to determine the total heat radiating from the flame, in which it is distributed as individual point sources along the flame centerline, weighted to be maximum at the widest point of the flame, about two thirds along the flame as illustrated in Fig. 19.
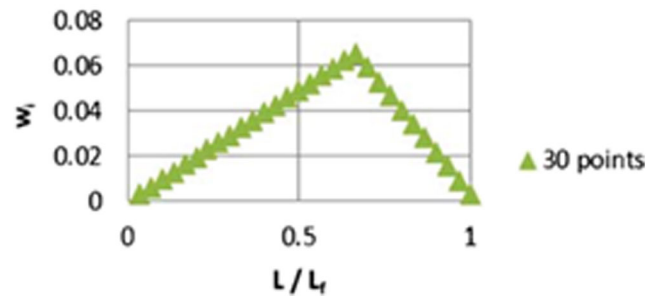
19 Distribution of radiant heat source along the flame centerline (Miller 2017)

Total heat radiating from the flame Q_R is determined using radiant heat fraction η from the Chamberlain correlation and it was found to be reasonable for the natural gas jet flame in a vertical and horizontal orientation. For hydrogen jet fire, the radiant heat fraction is correlated to mass flux at pipe exit, M_{flux}. The data is found to be well fitted for vertical hydrogen jet fire, but the value is higher for equivalent horizontal and 45° release hydrogen flames. This phenomenon occurs probably due to the reflection of thermal radiation off the ground between the flame and the point of measurement and/or the hot ground underneath the flame preheating some of the air entering the flame, increasing the flame temperature, and would diminish once the flame is elevated higher off the ground. In this case, a correction factor was applied where the equation is given as

$$\frac{\eta_H}{\eta_V} = 0.0764 \frac{L_c}{h_{RC}} + 1.3634 \tag{42}$$

where η_H is the radiant heat fraction in a horizontal orientation, η_V is the radiant heat fraction in a vertical orientation, L_c is the centerline flame length, and h_{RC} is the distance between the flame radiant center and the ground. For hydrogen/natural gas mixture jet fire, the η was found to be similar for 45° and horizontal jet flames at the same flow rates, while for the mixtures with the presence of an inert, radiative fraction, η increased as the content of inert increases (Fig. 20).

Later, a completely new dimensionless group has been introduced in generalizing the radiative fraction correlation, consisting of the flame Froude number, mass fraction of fuel at stoichiometric conditions, and the density ratio of fuel gas to ambient air to a radiative fraction (Zhou et al. 2018). The study covers hundreds of orifice exit diameters using a range of fuels (hydrogen, methane, and propane) at vertical and horizontal orientations, buoyancy- and momentum-dominated releases, and subsonic, sonic, and supersonic velocities. It was found that the capability exceeds previous correlation based on
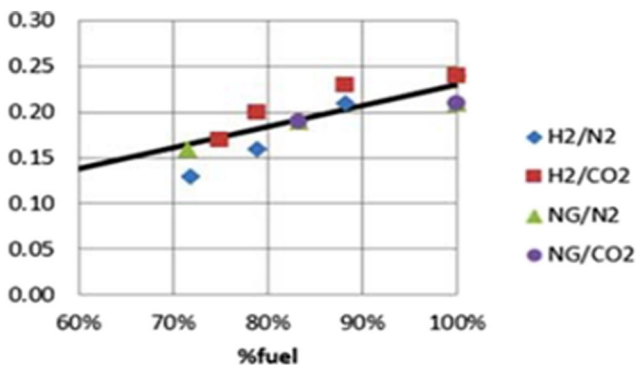

Fig. 20 Impact of inert addition in gas mixtures (Miller 2017)

Froude number only or the global residence time with/ without correction factors. The equation deduced from the theoretical analysis of the radiative fraction and yield is as follows

$$\eta f_s / \sqrt{\rho_s / \rho_\infty} \tag{43}$$

where η, f_s, ρ_s, and ρ_∞ are the radiant heat fraction, mass fraction of fuel at stoichiometric condition, gas density at the jet exit, and ambient air density, respectively. It must be noted again, in the semi-empirical models, that η is only accounted in PSM and MPSM. Meanwhile, for SFM and LSM, the radiative heat was assumed to totally depend on the flame shape configuration.

Atmospheric Conditions

The dispersion behavior of fuel released heavily depends on atmospheric conditions. This includes the wind speed, wind direction, ambient temperature, relative humidity, and ambient pressure. An experiment conducted by Hu et al. (2013b) on vertical propane jet fire characteristics in a reduced atmospheric pressure depicted that the mean flame height is higher in subatmospheric conditions as well as the flame lift-off height. This condition can be correlated to a fraction of stoichiometric air entrained, n_a, a basic parameter in the flame height correlation.

$$n_a = \text{mass of air entrained/mass of air reacted} \tag{44}$$

In their work, they prescribed, in normal atmospheric pressure, the value of $n = 9.6$; however, the value is 73% lower for subatmospheric pressure condition. The change of atmospheric pressure may have a direct effect on the flame height and lift-off height, giving higher value in reduced atmospheric pressure (Hu et al. 2013a). However, none of the models have ever considered the change of pressure as most of the jet fire occurrence was assumed to occur at normal atmospheric pressure. On another note, wind speed and wind direction are also held to have considerable effects on the jet fire characteristics particularly on flame shape and appearance as well as the heat distribution to the surrounding. This indirectly gives variation to the fraction of heat radiated η (Gómez-Mares et al. 2010). In a study conducted by Huang et al. (2017), wind speed can be correlated to the maximum flame width of jet flame geometrical properties. Clearly, it can be said that wind speed and direction give a direct effect to flame geometrical features, consequently the fraction of heat radiated to the surrounding in the case of free jet fire occurrence and thermal distribution to the surface impinged in the case of jet flame impingement.

All models, i.e., SFM, PSM, MPSM, and LSM, agreed that atmospheric transmissivity τ value also is very important. As

can be seen from Eq. (44), each model takes into account atmospheric transmissivity (τ) due to the absorbance of radiant heat through atmosphere intervention as it goes to the local recipient in every jet fire occasion (van der Bosch et al. 2005). It was a function of ambient temperature and relative humidity. The value was normally taken close to unity. It implies that the total heat released by the jet fire is not best representing heat received by the recipient and this would give an under- or overprediction on the total radiative heat to the receivers. van der Bosch et al. (2005) highlighted a method to determine the atmospheric transmissivity (τ) as

$$\tau = 1-\alpha_{\mathrm{w}}-\alpha_{\mathrm{c}} \tag{45}$$

where α_{w} is the water vapor absorption factor and α_{c} is the carbon dioxide absorption factor. Detailed calculation of water vapor absorption factor, α_{w}, and carbon dioxide absorption factor, α_{c}, has been detailed elsewhere (van der Bosch et al. 2005). Since water vapor and carbon dioxide are a major constituent in radiant heat wavelength that would reduce the absorption factor to be less than unity, thus the observation field plays some significant roles in the determination of the transmissivity value. The assumption might be true for measurement of distance at a small distance. However, it may provide an erroneous measurement at the far field. This is due to absorptivity of the radiative wave through major constituents of combustion products, carbon dioxide and water vapor; thus, it shall not be ignored particularly for far-field measurement.

On the other hand, atmospheric transmissivity value also can be expressed as a direct function of relative humidity, RH, and distance from the flame surface to the receiver, X, as mentioned elsewhere (Brzustowski et al. 1975; Palacios et al. 2012):

$$\tau = 0.79 \left(\frac{100}{\mathrm{RH}}\right)^{1/16} \left(\frac{30.5}{X}\right)^{1/16} \tag{46}$$

However, atmospheric transmissivity values available in the literature are generally different with the values given by research works. For example, the study performed by Hankinson and Lowesmith (2012) depicted that the value of τ depends on prevailing atmospheric conditions (temperature and humidity) as it is largely driven by carbon dioxide and water vapor in the atmosphere (Kohout and Turpin 2013). Some other studies made an assumption that the transmissivity term should be unity or close to unity (Gómez-Mares et al. 2010; Zhang et al. 2015). It was suggested that the value is taken as unity when the distance relative to the heat source is less than 10 m (UKOOA 2006). Another method that can be used to estimate the values of τ is by using equations found in Rohsenow et al. (1998). This method was applied by Gómez-

Mares et al. (2010) for a mass flow rate of 0.09–0.43 kg s^{-1} of propane, applying an SFM to obtain Q_R, and the estimated uncertainty is $\pm 3\%$ with 95% confidence level. However, the data of Q_R are scattered relative to the distance where the measurement is taken. This is due to the turbulence phenomenon and flame oscillation in far-field observations which has a direct influence on the sensor measured (Gómez-Mares et al. 2010). Sonju and Hustad (1984) reported quite a scattering results with 60% variation, higher than the variation obtained by Gómez-Mares et al. (2010).

It is interesting to note that the study of Molina et al. (2007) did not take into account the atmospheric transmissivity term for large-scale jet fires when the PSM was applied in their work. The absence of the τ term led to quite significant differences in predicting the radiation value due to the fact that the energy is absorbed by the atmosphere at larger distance measurement. Later, it was found that the term could only be omitted at smaller distances (say, less than 3 m), where it was typically used in the experimental setup. From the experimental point of view, it was found that less radiant energy is lost to the atmosphere; thus, the transmissivity value is nearly unity (Hankinson and Lowesmith 2012). A work done by Mousavi and Parvini (2016) on the study of effective factors on leakage-induced hydrogen jet fire found a large variation in radiation heat measurement and suspected that leakage diameter, release pressure, and release height are the contributing parameters as compared to humidity and ambient temperature which have less significant effect. However, it is advisable to be careful when applying the transmissivity term to estimate the radiation heat at the larger-scale jet fire or measurement taken from far-field observation (Molina et al. 2007). An abnormal atmospheric condition in terms of relative humidity should also be taken into account as it poses a possible deviation from the true measurement of incident radiation. As a summary, it can be said that consideration of atmospheric transmissivity is independent relative to the type of model used but largely driven by the relative distance of the recipient.

Conclusion and Future Direction

This review has highlighted the governing parameters to determine radiant heat intensity from various jet release scenarios, different orientations, and scale of release and how the predictive models consider the important parameter in their model in order to give reliable and realistic results. The state of our knowledge about semi-empirical models used to estimate radiation heat from jet fire phenomena as revealed in this review suggests that there is still a long way to go before we can predict with any confidence. The following conclusions and future directions can be drawn from the analysis:

(i)   No general quantitative model is available to best predict the heat radiation from the jet fire in near- or far-field scenarios. This is hindered by several factors: (a) scale of the jet fire (small, medium, large), (b) distance from which the measurement is taken (near and far field), (c) jet fire orientation, and (d) other external factors such as geographical conditions.

(ii) For radiation estimation within a near-field observation, estimation given by the SFM and LSM appears to be more realistic as they consider the flame shape orientation and, hence, it provides better emissivity value. In general, cylindrical shape is the most common shape used to represent the flame shape in a vertical orientation, while other studies suggested rectangle and kite shapes to best represent the flame shape in a horizontal orientation. It was also found that the combination of flame shape has received little consideration although it could give a good approximation of flame surface. Thus, in a newly developed model LSM, a combination of flame shape has been studied and it was found that kite shape with the inclusion of lift-off best represents the flame shape for medium-scale jet flame in a horizontal orientation. However, more data is needed to close its application for small- and large-scale jet flame. For vertical jet fire, it was found that back-to-back cone fits the small jet flame and the combination of cone in the lower region and of cylinder in the upper region fits relatively the large-scale jet flame. It is also suggested to include the effects of flame with low luminosity such as hydrogen to the applicability of LSM.

(iii) There are two common types of MPSM: weighted MPSM and simple MPSM. In the near-field observation, weighted MPSM is more suitable to be used as compared to simple MPSM for jet fire in a vertical orientation, while in the far-field observation, the behavior of the weighted MPSM approximate to PSM indicates that weighted MPSM is suitable for both near- and far-field observations.

(iv) Due to the deformation of jet flame that can be caused by external factors such as wind speed, it resulted in an underestimation of radiant heat release up to 40%. Thus, consideration of the buoyancy region has been taken care of with the suggested method of the 1D flame integral model and the AP flame model. For jet flame with only buoyancy-dominated region, the projected length L_P should be measured as a function of nozzle width.

(v)   The PSM is more suitable to be used in far-field observation and the MPSM seems to give a realistic value considering the jet fire with buoyancy effects.

(vi) Although LSM is a newly developed model, the prediction of radiant heat gives encouraging result

relative to the validity of the model system. It does yield the expected values not only for near-field but also for far-field incident radiation, making this model usable in all practical situations. However, the challenge of using this model is that more data is required to ensure the validity and wider application for different fire orientations and scales.

Compliance with Ethical Standards

Conflict of Interest The authors declare that they have no conflict of interest.

Publisher's Note Springer Nature remains neutral with regard to jurisdictional claims in published maps and institutional affiliations.

References

Bagster DF, Schubacht SA (1996) The prediction of jet-fire dimensions. J Loss Prev Process Ind 9(3):241–245

Baillie S, Caulfield M, Cook DK, Docherty P (1998) A phenomenological model for predicting the thermal loading to a cylindrical vessel impacted by high pressure natural gas jet fires. Trans Inst Chem Eng 76(Part B):11

Becker HA, Liang D (1978) Visible length of vertical free turbulent diffusion flames. Combust Flame 32:115–137

Birch AD, Brown DR, Dodson MG, Swaffield F (1984) The structure and concentration decay of high pressure jets of natural gas. Combust Sci Technol 36(5–6):249–261

Bosch CJH, Weterings RAPM, Duijm NJ, Bakkum EA, Mercx WPM, Berg ACVD, Engelhard WFJM, Doormaal JCAMV, Wees RMMV (2005) Methods for the calculation of physical effects

Bradley D, Gaskell PH, Gu X, Palacios A (2016) Jet flame heights, lift-off distances, and mean flame surface density for extensive ranges of fuels and flow rates. Combust Flame 164:400–409

Brzustowski T, Gollahalli S, Gupta M, Kaptein M, Sullivan H (1975) Radiant heating from flares. *ASME paper*, (75-HT), 4

Chamberlain GA (1987) Developments in design methods for predicting thermal radiation from flare. Chem Eng Res Des 65(4):299–309

Crocker WP, Napier DH 1988 Mathematical models for the prediction of thermal radiation from jet fires. I.ChemE. Symposium Series No. 110, 331–347

Dadashzadeh M, Khan F, Hawboldt K, Amyotte P (2013) An integrated approach for fire and explosion consequence modelling. Fire Saf J 61:324–337

Ekoto IW, Ruggles AJ, Creitz LW, Li JX (2014) Updated jet flame radiation modeling with buoyancy corrections. Int J Hydrog Energy 39(35):20570–20577

Geankoplis, C. J. (2003). Transport processes and separation process principles: (includes unit operations). Prentice Hall Professional Technical Reference

Gómez-Mares M, Muñoz M, Casal J (2010) Radiant heat from propane jet fires. Exp Thermal Fluid Sci 34(3):323–329

Gopalaswami N, Liu Y, Laboureur DM, Zhang B, Mannan MS (2016) Experimental study on propane jet fire hazards: comparison of main

geometrical features with empirical models. J Loss Prev Process Ind 41:365–375

Hankinson G, Lowesmith BJ (2012) A consideration of methods of determining the radiative characteristics of jet fires. Combust Flame 159(3):1165–1177

Hankinson G, Lowesmith BJ, Evans JA, Shirvill LC (2007) Jet fires involving releases of crude oil, gas and water. Process Saf Environ Prot 85(B3):221–229

Hawthorne WR, Weddell DS, Hottel HC (1949) Mixing and combustion in turbulent gas jets. Combustion flame and explosions phenomena, p 266–288

Hu L, Wang Q, Delichatsios M, Tang F, Zhang X, Lu S (2013a) Flame height and lift-off of turbulent buoyant jet diffusion flames in a reduced pressure atmosphere. Fuel 109:234–240

Hu L, Wang Q, Tang F, Delichatsios M, Zhang X (2013b) Axial temperature profile in vertical buoyant turbulent jet fire in a reduced pressure atmosphere. Fuel 106:779–786

Huang Y, Li Y, Dong B, Li J (2017) Predicting the main geometrical features of horizontal rectangular source fuel jet fires. J Energy Inst:1–11

Institute, A. P (2008) ISO 23251 (identical) petroleum and natural gas industries, Pressure-relieving and depressuring systems. API Publishing Services, Washington, D.C

Johnson AD, Brightwell HM, Carsley AJ (1994) A model for predicting the thermal radiation hazards from large-scale horizontally released natural gas jet fires. IChemE Symposium Series No. 134

Jujuly MM, Rahman A, Ahmed S, Khan F (2015) LNG pool fire simulation for domino effect analysis. Reliab Eng Syst Saf 143:19–29

Kalghatgi GT (1983) The visible shape and size of a turbulent hydrocarbon jet diffusion flame in a cross-wind. Combust Flame 52:91–106

Kalghatgi GT (2010) Lift-off heights and visible lengths of vertical turbulent jet diffusion flames in still air. Combust Sci Technol 41:17–29

Kiran DY, Mishra DP (2007) Experimental studies of flame stability and emission characteristics of simple LPG jet diffusion flame. Fuel 86(10–11):1545–1551

Kohout A, Turpin T (2013) Recommended parameters for solid flame models for land based liquefied natural gas spills, Office of energy projects. Federal Energy Regulatory Commission, Washington, DC

Kozanoglu B, Zárate L, Gómez-Mares M, Casal J (2011) Convective heat transfer around vertical jet fires: an experimental study. J Hazard Mater 197:104–108

Laboureur DM, Gopalaswami N, Zhang B, Liu Y, Mannan MS (2016) Experimental study on propane jet fire hazards: assessment of the main geometrical features of horizontal jet flames. J Loss Prev Process Ind 41:355–364

Lowesmith BJ, Hankinson G (2012) Large scale high pressure jet fires involving natural gas and natural gas/hydrogen mixtures. Process Saf Environ Prot 90(2):108–120

Lowesmith BJ, Hankinson G (2013) Large scale experiments to study fires following the rupture of high pressure pipelines conveying natural gas and natural gas/hydrogen mixtures. Process Saf Environ Prot 91(1–2):101–111

Lowesmith BJ, Hankinson G, Acton MR, Chamberlain G (2007) An overview of the nature of hydrocarbon jet fire hazards in the oil and gas industry and a simplified approach to assessing the hazards. Process Saf Environ Prot 85(B3):207–220

Lyons KM (2007) Toward an understanding of the stabilization mechanisms of lifted turbulent jet flames: experiments. Prog Energy Combust Sci 33(2):211–231

Markstein GH, Ris JD (1990) Wall-fire radiant emission. Part 1: slot-burner flames, comparison with jet flames. Twenty-Third Symposium (International) on Combustion/The Combustion Institute, p 1685–1692

Mccaffrey BJ (1989) Momentum diffusion flame characteristics and the effects of water spray. Combust Sci Technol 63(4–6):315–335

Miller D (2017) New model for predicting thermal radiation from flares and high pressure jet fires for hydrogen and syngas. Process Saf Prog 36(3):237–251

Mogi T, Horiguchi S (2009) Experimental study on the hazards of high-pressure hydrogen jet diffusion flames. J Loss Prev Process Ind 22(1):45–51

Molina A, Schefer RW, Houf WG (2007) Radiative fraction and optical thickness in large-scale hydrogen-jet fires. Proc Combust Inst 31:2565–2572

Molkov V, Saffers J-B (2013) Hydrogen jet flames. Int J Hydrog Energy 38(19):8141–8158

Mousavi J, Parvini M (2016) Analyzing effective factors on leakage-induced hydrogen fires. J Loss Prev Process Ind 40:29–42

Palacios A, Casal J (2011) Assessment of the shape of vertical jet fires. Fuel 90(2):824–833

Palacios Rosas A (2011) Study of jet fires geometry and radiative features. Doctor of Philosophy, Universitat Politècnica de Catalunya

Palacios A, Muñoz M, Casal J (2009) Jet fires: an experimental study of the main geometrical features of the flame in subsonic and sonic regimes. AICHE J 55(1):256–263

Palacios A, Munoz M, Darbra RM, Casal J (2012) Thermal radiation from vertical jet fires. Fire Saf J 51:93–101

Palacios A, Bradley D, Hu L (2016) Lift-off and blow-off of methane and propane subsonic vertical jet flames, with and without diluent air. Fuel 183:414–419

Peter N, Williams FA (1983) Liftoff characteristics of turbulent jet diffusion flames. Am Inst Aeronaut Astronaut J 21(3):423–429

Raj PK (2007) LNG fires: a review of experimental results, models and hazard prediction challenges. J Hazard Mater 140:444–464

Rajendram A, Khan F, Garaniya V (2015) Modelling of fire risks in an offshore facility. Fire Saf J 71:79–85

Rohsenow, W. M., Hartnett, J. R. and Cho, Y. I. (1998). Handbook of heat transfer. (Third edition). McGraw-Hill Companies

Røkke NA, Hustad JE, Sønju OK (1994) A study of partially premixed unconfined propane flames. Combust Flame 97(1):88–106

Santos A, Costa M (2005) Reexamination of the scaling laws for Nox emissions from hydrocarbon turbulent jet diffusion flame. Combust Flame 142:160–169

Schefer R, Houf B, Bourne B, Colton J (2004) Experimental measurements to characterize the thermal and radiation properties of an open-flame hydrogen plume. 15th NHA Meeting, p 26–30

Schefer RW, Houf WG, Williams TC, Bourne B, Colton J (2006) Characterization of high-pressure, underexpanded hydrogen-jet flame. Int J Hydrog Energy 32:2081–2093

Sivathanu YR, Gore JP (1993) Total radiative heat loss in jet flames from single point radiative flux measurements. Combust Flame 94:265–270

Smith T, Periasamy C, Baird B, Gollahalli SR (2005) Trajectory and characteristics of buoyancy and momentum dominated horizontal jet flames from circular and elliptic burners. J Energy Resour Technol 128:300–310

Sonju OK, Hustad J (1984) An experimental study of turbulent jet diffusion flames. Am Inst Aeronaut Astronaut J

Studer E, Jamois D, Jallais S, Leroy G, Hebrard J, Blanchetière V (2009) Properties of large-scale methane/hydrogen jet fires. Int J Hydrog Energy 34(23):9611–9619

Sugawa O, Sakai K (1996) Flame length and width produced by ejected propane gas fuel from a pipe. Int Assoc Fire Saf Sci:411–421

Suris AL, Flankin EV, Shorin SN (1978) Length of free diffusion flame. Combust Explosion Shock Waves 13(4):459–462

Tao C, Shen Y, Zong R (2016) Experimental determination of flame length of buoyancy-controlled turbulent jet diffusion flames from inclined nozzles. Appl Therm Eng 93:884–887

UKOOA (2006) Fire and explosion guidance. Part 2: avoidance and mitigation of fires

Wang Q, Hu L, Zhang M, Tang F, Zhang X, Lu S (2014) Lift-off of jet diffusion flame in sub-atmospheric pressures: an experimental investigation and interpretation based on laminar flame speed. Combust Flame 161(4):1125–1130

Wertenbach HG (1971) Spread of flames on cylindrical tanks for hydrocarbon fluids. Gas Erdgas 112(8)

Zhang B, Liu Y, Laboureur D, Mannan MS (2015) Experimental study on propane jet fire hazards: thermal radiation. Ind Eng Chem Res 54(37):9251–9256

Zhang X, Hu L, Zhang X, Tang F, Jiang Y, Lin Y (2017) Flame projection distance of horizontally oriented buoyant turbulent rectangular jet fires. Combust Flame 176:370–376

Zhou K, Jiang J (2016) Thermal radiation from vertical turbulent jet flame: line source model. J Heat Transf 138(4):042701

Zhou K, Liu J, Jiang J (2016) Prediction of radiant heat flux from horizontal propane jet fire. Appl Therm Eng 106:634–639

Zhou K, Qin X, Wang Z, Pan X, Jiang J (2018) Generalization of the radiative fraction correlation for hydrogen and hydrocarbon jet fires in subsonic and chocked flow regimes. Int J Hydrog Energy 43(20): 9870–9876